Atlas-Based Whole-Body PET-CT Segmentation Using a Passive Contour Distance

Fabian Gigengack[1,2], Lars Ruthotto[3], Xiaoyi Jiang[2], Jan Modersitzki[3], Martin Burger[4], Sven Hermann[1], and Klaus P. Schäfers[1]

[1] European Institute for Molecular Imaging (EIMI), University of Münster, Germany
[2] Department of Mathematics and Computer Science, University of Münster, Germany
[3] Institute of Mathematics and Image Computing, University of Lübeck, Germany
[4] Institute for Computational and Applied Mathematics, University of Münster, Germany

Abstract. In positron emission tomography (PET) imaging, the segmentation of organs is necessary for many quantitative image analysis tasks, e.g., estimation of individual organ concentration or partial volume correction. To this end we present a fully automated approach for whole-body segmentation which enables large-scale and reproducible studies. The approach is based on joint segmentation and atlas registration. The classical active contour approach by Chan and Vese is modified to a novel *passive contour* energy term with implicitly incorporated information about shape and location of the organs. This new energy is added to a registration functional which is based on both functional (PET) and morphological (CT) data. The proposed method is applied to medical data, given by 13 PET-CT data sets of mice, and quantitatively compared to manually drawn VOIs. An average Dice coefficient of 0.73 ± 0.10 for the left ventricle, 0.88 ± 0.05 for the bladder, and 0.76 ± 0.07 for the kidneys shows the high accuracy of our method.

Keywords: Segmentation, Active Contour, Passive Contour, Registration, Atlas, PET-CT, Whole-Body.

1 Introduction

Positron emission tomography (PET) is widely used in medical imaging to assess functional information in the body. However, quantitative evaluation of PET images is challenging due to the rather limited spatial resolution and low signal-to-noise ratio which makes the segmentation of organs necessary for various applications. Estimating organ concentration in biodistribution studies [6], [9], or analyzing organ specific diseases such as myocardial infarction demands for an adequate whole-body segmentation. In addition, organ segmentation is mandatory for many partial volume correction techniques [15]. To this end we developed a general approach for whole-body segmentation based on joint segmentation and registration.

B.H. Menze et al. (Eds.): MCV 2012, LNCS 7766, pp. 82–92, 2013.

1.1 Related Work

Many approaches originating from computer vision are transferred to medical imaging as they are well understood and, at the same time, also efficiently applicable to volumetric (3D) medical images. A popular approach in computer vision for automatic segmentation is active contours as introduced by Chan and Vese [2]. The method was successfully applied to medical imaging based on brain MRI data [3]. The main idea of active contours is also exploited in our work, but in a reversed interpretation, cf. Sec. 2.

There is a large demand for automatic segmentation in medical imaging as the manual segmentation of organs is time-consuming for 3D data sets. Further, inter- and intra-observer variability can have a high impact. This is why manual segmentation is inapplicable for large-scale and reproducible studies. We restrict the following discussion to related literature on segmentation of PET and CT and joint registration and segmentation.

An automated method for whole-body segmentation in Micro-CT data of mice was introduced by Baiker et al. [1]. The approach consists of a model-based registration with a subsequent intensity-based registration. They achieved high accuracies for skin and skeleton. However, they did not report results for inner organs which are the focus of this work. This might be due to the low soft tissue contrast of the CT images which makes the localization of inner organs challenging. We overcome this limitation (inter alia) by using functional information in terms of PET images (and additional CT images).

Wang et al. presented a registration approach based on a statistical shape model for small-animal PET segmentation [13]. High uptake organs guide the registration using a conditional Gaussian model and allow good estimates for low uptake organs as well. However, for the labeling of organs the method requires user interaction.

Recently various techniques were published combining registration and segmentation. A taxonomy on this topic is given in [8]. A method, which is basically similar to our proceeding, was presented by Yezzi et al. [14]. They propose a variational framework that uses active contours for segmentation with a simultaneous registration of features. The level-set based segmentation separates only one object from the background which makes this method inapplicable for multiple organ segmentation tasks. Further, only rigid and affine transformations were practically explored.

2 Methods

In this paper we present a novel atlas-based segmentation approach. The general scheme is illustrated in Fig. 1. Given a pair of spatially aligned PET and CT images (real data on the left of Fig. 1) of the same subject, we follow a two-step strategy. After aligning the atlas (atlas data on the right of Fig. 1) and the real data with an affine transformation, a tailored registration functional with joint segmentation is minimized. Three distance terms drive the registration: 1. Distance of the atlas CT and real CT, 2. Distance of the atlas PET and real PET,

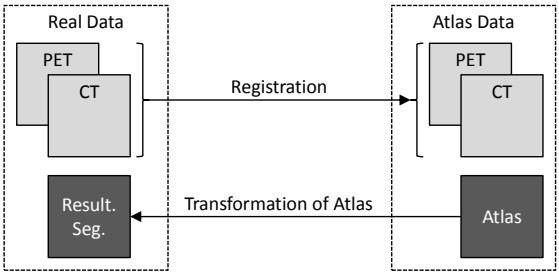

Fig. 1. General scheme: The inverse of the estimated transformation is applied to the atlas to segment the real data

3. Segmentation distance motivated by Chan and Vese [2]. Instead of matching a contour to the data, the novel segmentation distance is used to optimize for the transformation that aligns the data best to the (passive) contours. This turns around the interpretation of standard active contours models. Finally, the atlas organ definitions are transformed with the inverse transformation and yield the resulting segmentation of the real data, cf. bottom of Fig. 1.

In particular, we address the following points:

1. Transition of 2D active contours to 3D passive contours for medical image segmentation
2. Fully automation to make large-scale studies possible (user interaction is time-consuming)
3. Non-rigidity of atlas-based whole-body segmentation
4. Multimodality treatment (function and morphology)
5. Handling of multiple organs for joint registration and segmentation

2.1 Joint Passive Contour Segmentation and Registration

As a technical preprocessing step, a rough alignment of the atlas dataset and the real dataset is performed by matching the atlas CT to the real CT with an affine transformation to overcome differences in the orientation, scaling, and translation. As both images are of the same modality we choose the sum of squared differences (SSD) distance measure.

To overcome anatomical variations of organs, the information of the PET and the CT images is used simultaneously in a joint registration functional. Hence, anatomical and functional information is exploited at the same time. In addition, we include a novel segmentation distance term into the functional, inspired by Chan and Vese [2]. The Chan-Vese distance measures the in-class variance according to the atlas organ definitions. We derive the complete registration model by first looking at standard image registration for the CT images.

For the alignment of the CT images, the real data $\mathcal{T}_{CT} : \Omega \to \mathbb{R}$ (template image) is registered to the atlas CT image $\mathcal{R}_{CT} : \Omega \to \mathbb{R}$ (reference image), where

$\Omega \subset \mathbb{R}^3$ is the image domain. The output of the registration is a transformation $y : \mathbb{R}^3 \to \mathbb{R}^3$ representing point-to-point correspondences between $\mathcal{T}_{CT}$ and $\mathcal{R}_{CT}$. To find y, the following functional has to be minimized

$$\min_y \left\{ \mathcal{D}^{\text{SSD}}(\mathcal{T}_{CT} \circ y,\ \mathcal{R}_{CT}) + \alpha_{\mathcal{S}} \cdot \mathcal{S}(y) \right\} . \tag{1}$$

$\mathcal{D}^{\text{SSD}}$ is the SSD distance functional and $\alpha_{\mathcal{S}} \in \mathbb{R}^+$ is a weighting factor of the regularization functional $\mathcal{S}$. By using regularized spline image interpolation we reduce artifacts in the PET images which justifies the usage of the SSD measure.

We assume that the PET and corresponding CT measurement approximately share the same geometry and hence y can be used to align both modalities. In practice the images provide complementary information which motivates the exploration of both modalities in a joint registration functional. The CT images guide the registration whereas the PET images provide important information in soft tissue regions. As the scanned mice are anesthetized the spatial variations are kept to a minimum. However, changes due to, e.g., bladder filling, are possible.

Our joint registration functional is an extension of (1) by adding a term for the PET data and an additional passive contour term $\mathcal{D}_{PC}$

$$\begin{aligned} \min_y \{\ \alpha_{CT} \cdot \mathcal{D}^{\text{SSD}}(\mathcal{T}_{CT} \circ y,\ \mathcal{R}_{CT}) + \alpha_{PET} \cdot \mathcal{D}^{\text{SSD}}(\mathcal{T}_{PET} \circ y,\ \mathcal{R}_{PET}) \\ + \alpha_{PET}^{PC} \cdot \mathcal{D}_{PC}(\mathcal{T}_{PET} \circ y,\ A) + \alpha_{\mathcal{S}} \cdot \mathcal{S}(y)\ \} , \end{aligned} \tag{2}$$

where $\mathcal{T}_{PET}, \mathcal{R}_{PET} : \Omega \to \mathbb{R}$ are the real PET image and the atlas PET image. $\alpha_{CT}, \alpha_{PET}, \alpha_{PET}^{PC}, \alpha_S \in \mathbb{R}^+$ are weighting factors for the individual distance functionals and are discussed later. $\mathcal{D}_{PC}$ is the passive contour distance and A denotes the delineation of the atlas organs.

Passive Contour Distance. Let us now derive the passive contour term $\mathcal{D}_{PC}$. The classical Chan-Vese functional [2] is defined as follows

$$\mathcal{CV}(C) = \int_{C^{in}} (\mathcal{T}(x) - \mu(\mathcal{T}, C^{in}))^2\ dx + \int_{C^{ex}} (\mathcal{T}(x) - \mu(\mathcal{T}, C^{ex}))^2\ dx\ . \tag{3}$$

The function μ computes an average value of $\mathcal{T}$ (we omit the subscript for simplicity) according to the interior (C^{in}) respectively the exterior (C^{ex}) of the contour C. The aim is to find the (active) contour C that minimizes the energy $\mathcal{CV}(C)$. We can rewrite this formulation as a functional of the transformation y

$$\mathcal{CV}(y) = \int_{y(\Omega)} (\mathcal{T}(x) - \mu(\mathcal{T},\ A \circ y;\ x))^2\ dx\ . \tag{4}$$

$\mu(\mathcal{T},\ A \circ y;\ \cdot\ )$ is constant inside each organ containing the average intensity of $\mathcal{T}$ over the respective segment. A simple 2D example to illustrate the function μ is given in Fig. 2.

The atlas definitions A in Fig. 2(b) exactly match the contours of the blurred and noisy input image (a). By applying the segmentation function μ we result in a recovered image without noise and blur (c).

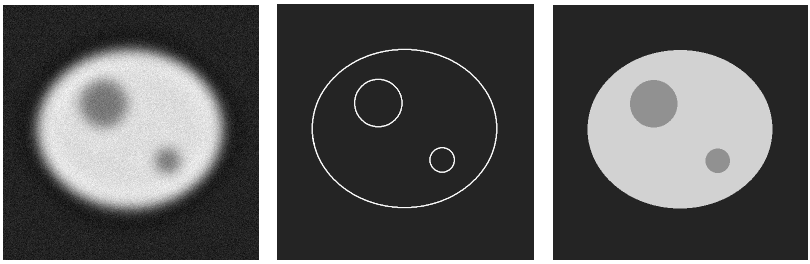

(a) Input image $\mathcal{T}$ (b) Atlas definitions A (c) $\mu(\mathcal{T},\ A;\ \cdot\,)$

Fig. 2. Illustration of μ (2D). Given the image $\mathcal{T}$ (left) and the atlas definitions A (middle) we can apply the segmentation function $\mu(\mathcal{T},\ A;\ \cdot\,)$ (right).

By substitution $x \to y(x)$ in (4) we receive

$$\mathcal{CV}(y) = \int_{\Omega} (\mathcal{T}(y(x)) - \mu(\mathcal{T} \circ y,\ A;\ x))^2 \cdot |\det(\nabla y(x))|\, dx\ . \tag{5}$$

The term $\mathcal{D}_{PC}$ is then defined as:

$$\mathcal{D}_{PC}(\mathcal{T} \circ y,\ A) := \frac{1}{2} \int_{\Omega} (\mathcal{T}(y(x)) - \mu(\mathcal{T} \circ y, A; x))^2 \cdot \det(\nabla y(x)) dx\ . \tag{6}$$

Thus, by finding an adequate transformation y the in-class variance of $\mathcal{T} \circ y$ according to the atlas A is minimized. Note that we can drop the absolute value bars for the Jacobian determinant, if the transformation is diffeomorphic, cf. Sec. 2.2.

Instead of adjusting the contour to the data (active contour, analogously deformable templates), the data is adjusted to the contour (passive contour) in our case. Hence we have an optimization problem in the transformation y and not in the contour. This allows us directly to treat multiple segments at once and not only to separate one foreground object from the background (note that there exist also active contour approaches for multiple segments [12]). A further advantage of passive contours compared to active contours is the implicitly incorporated information about shape and location of the organs. In contrast to active contours, contours can not split in multiple objects. Further, active contour approaches require proper initialization. In our case the initialization of the passive contours is directly given by the atlas definitions. Furthermore, the fixed integration domain for segmentation simplifies computations compared to exiting atlas-based segmentation methods.

2.2 Regularization

The non-rigid nature of whole-body segmentation poses challenges to the estimation of the transformation y. To guarantee diffeomorphic transformations

and to be highly robust against noise, we utilize hyperelastic regularization [5]. The regularization functional $\mathcal{S}$ controls changes in length and volume of the transformation y. The weighting factor $\alpha_{\mathcal{S}}$ in (2) is thus a compact notation for the weighting of two regularization terms.

Local adaptive regularization prevents unphysiological contraction or expansion of organs. The organ definitions are given by our atlas organ delineations A. The areas inside organs get a higher volume regularization value $(2 \cdot 10^5)$ compared to normal body tissue $(1 \cdot 10^5)$ which keeps volumetric changes inside organs to a minimum.

2.3 Evaluation

The resulting segmentations are compared to manually drawn VOIs. The Dice coefficient is used to quantitatively compare our segmentation to the ground-truth. For two sets X and Y the Dice coefficient is defined as $D(X,Y) = \frac{2|X \cap Y|}{|X|+|Y|}$.

To assess whether the registration algorithm performs successful or not we analyze the Jacobian determinant. It specifies the volumetric change due to the transformation. A value of 1 represents no volumetric change and a value smaller (greater) than 1 indicates compression (expansion). For positive values the transformations are diffeomorphic. Fig. 4 shows a distribution of the Jacobian for all results.

2.4 Implementation

The implementation is based on the FAIR registration toolbox [10] in MATLAB®. In a first step the images are brought to the same resolution (voxel size of 0.35 mm). We use a multi-level strategy with a scaling of 0.5 between two adjacent levels, starting with a resolution of $16 \times 10 \times 40$ (voxel size of 2.77 mm) and going to a final resolution of $64 \times 40 \times 160$ (voxel size of 0.69 mm). Optimization is performed with a Gauss-Newton scheme in combination with a PCG solver for the linear system of equations, cf. [10]. Spline interpolation is used along with a regularization of the moments. The parameter controlling the amount of regularization is chosen to be 1 for the affine pre-registration and 0.5 for the joint registration. The regularization for the affine pre-registration is higher to reduce the amount of details in the images for the rough alignment.

3 Experimental Results

3.1 Data

This work is based on ^{18}F-FDG-PET/CT data of 13 healthy adult C57/Bl6 mice (without any intervention), representing the most widely used radiotracer and mouse strain in preclinical PET studies.

PET experiments were carried out using a high resolution (0.7 mm full width at half maximum) small animal scanner (32 module quadHIDAC, Oxford Positron Systems Ltd., Oxford, UK) with uniform spatial resolution over a large

cylindrical field-of-view (165 mm diameter, 280 mm axial length). Mice were anesthetized with oxygen/isoflurane inhalation (2% isoflurane, 0.4 l/min oxygen) and body temperature was maintained at physiological values by a heating pad. One hour after intravenous injection of 10 MBq ^{18}F-FDG in 100 µl 0.9% saline list-mode data were acquired for 15 min. Subsequently, the scanning bed was transferred to the CT scanner (Inveon, Siemens Medical Solutions, USA) and a CT acquisition with a spatial resolution of ∼80 µm was performed for each mouse after intravenous injection of a contrast agent. The reconstructed image data sets were aligned with a rigid transformation based on extrinsic markers attached to the scanning bed and the image analysis software (Inveon Research Workplace 3.0, Siemens Medical Solutions, USA).

3.2 Atlas

The Digimouse software phantom [4] serves as an atlas. The organ delineations of the pixel atlas are filled with realistic values according to our scanning protocol to construct a pseudo-PET and pseudo-CT phantom image. This has to be done only once in advance. The resulting images are spatially aligned phantom images with a known ground-truth segmentation. No blurring or noise is added to the images.

For the heart, the used ^{18}F-FDG tracer accumulates mainly in the left ventricle. As Digimouse provides only a combined segment for the whole heart (including left and right ventricle and the blood pool) we apply some minor modifications, see Fig. 3. The heart region of the atlas is replaced by a manual threshold segmentation of the left ventricle using the accompanied Digimouse PET data. In addition, the bladder is slightly moved in posterior direction to better fit our real data (this stabilizes the transformation estimation by minimizing the local average deformation). The original image is shown in Fig. 3(a) and the modified version in (b).

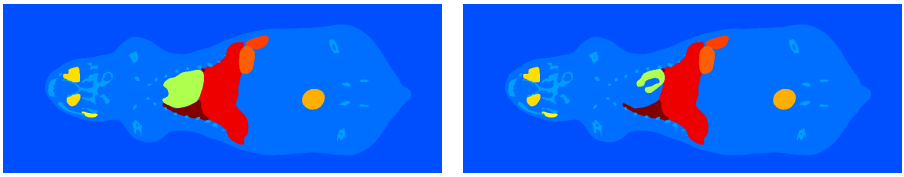

(a) Original atlas (b) Modified atlas

Fig. 3. The heart's segmentation (green area) and the bladder (orange area) in the original version of the Digimouse phantom (a) is replaced in the modified atlas (b) to better match the real data

3.3 Results

For the non-parametric registration, the following approach is used to provide meaningful values for the various parameters in (2). An exhaustive parameter

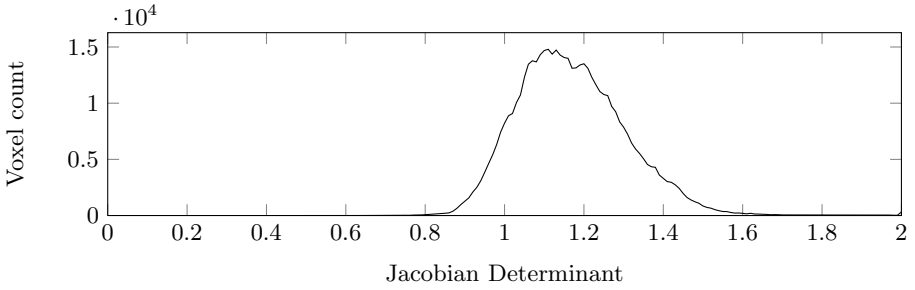

Fig. 4. Summed histograms of the Jacobian determinant of all data set

Table 1. Dice coefficients of the 13 mice for the heart (left ventricle), bladder and kidneys

Mouse	1	2	3	4	5	6	7	8	9	10	11	12	13	Avg.	Std.
Heart	0.85	0.84	0.84	0.85	0.79	0.62	0.77	0.72	0.60	0.60	0.68	0.60	0.75	0.73	0.10
Bladder	0.90	0.88	0.78	0.91	0.92	0.88	0.93	0.92	0.93	0.79	0.86	0.82	0.87	0.88	0.05
Kidneys	0.83	0.63	0.80	0.82	0.73	0.65	0.66	0.83	0.80	0.73	0.80	0.78	0.84	0.76	0.07
Avg.	0.86	0.78	0.81	0.86	0.81	0.72	0.79	0.82	0.77	0.71	0.78	0.74	0.82		
Std.	0.04	0.13	0.03	0.05	0.10	0.14	0.14	0.10	0.17	0.10	0.09	0.11	0.06		

search is performed for a randomly selected mouse. For each parameter combination the estimated segmentation is compared to the manual segmentation. The estimation giving the best fit is declared as the optimal parameter set for all experiments as they follow all the same protocol. We found the following optimal parameter set: $\alpha_{CT} = 10$, $\alpha_{PET} = 10$, $\alpha_{PET}^{PC} = 100$. For the hyperelastic regularization we found an optimal weighting for the length term of 1000 and for the volumetric regularization we refer to the regularization paragraph in Sec. 2.2.

For all transformations, the Jacobian determinant is everywhere positive and centered around 1, see Fig. 4. The global minimum is 0.26 and the global maximum is 2.66 which implicates diffeomorphisms. Note that the small shift of the maximum peak to a value greater than 1 in Fig. 4 is due to the affine component of the transformations indicating that the atlas is on average a little bit bigger than the real mice.

For all datasets an average Dice coefficient of 0.73 ± 0.10 could be achieved for the left ventricle, 0.88 ± 0.05 for the bladder, and 0.76 ± 0.07 for the kidneys. The estimated segmentation for one mouse is exemplified in Fig. 5. The Dice coefficients for all analyzed organs and mice can be found in Table 1.

The improvement due to our new passive contour distance can be assessed by setting $\alpha_{PET}^{PC} = 0$ and thus disabling the segmentation input. The objective is to analyze whether the additional passive contour distance can even improve the high accuracy of our multimodal PET-CT registration functional alone. For $\alpha_{PET}^{PC} = 0$, the Dice coefficient for the left ventricle was 0.61 ± 0.12, for the bladder 0.80 ± 0.07, and for the kidneys 0.76 ± 0.08. This means an improvement

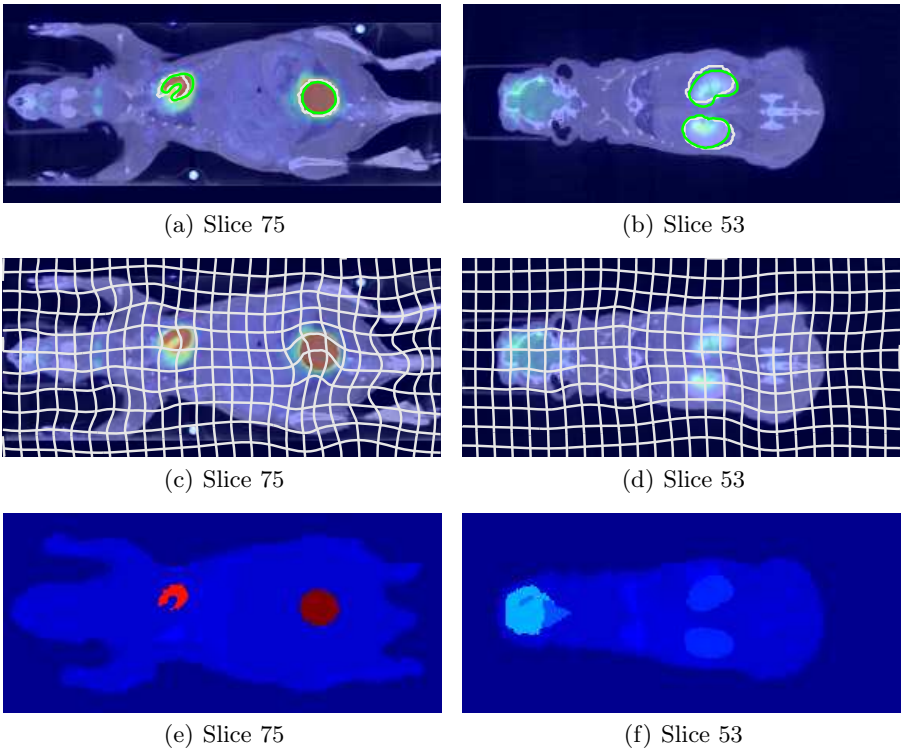

(a) Slice 75 (b) Slice 53

(c) Slice 75 (d) Slice 53

(e) Slice 75 (f) Slice 53

Fig. 5. Visualization of 3D registration results for whole-body segmentation. Overlay of 2D projections of PET, CT and contours ((a) heart and bladder, (b) kidneys) and transformation grid y_{opt} ((c), (d)). The estimated segmentations are plotted with white contours and the ground-truth segmentation is shown in green. The estimated contour of the body is plotted for additional visual assessment of the registration accuracy. Slices of the piecewise constant approximations $\mu(\mathcal{T}_{PET} \circ y_{opt}, A)$ are shown in (e) and (f).

of 16% for the left ventricle and 9% for the bladder. We found no improvement for organs with relatively low uptake like the kidneys.

4 Conclusion and Future Work

A novel fully automated approach for whole-body segmentation of PET data is presented in this work. The centerpiece of the proposed joint segmentation and registration method is the introduction of a novel segmentation distance for registration inspired by Chan and Vese [2]. As the interpretation is reversed to active contour models, we denote this as passive contours. Further, the registration is performed based on functional and morphological data simultaneously.

A validation based on the Dice coefficient and the Jacobian determinant demonstrates the high accuracy of our method. Further, the benefit of the

additional Chan-Vese distance, in contrast to multimodal PET-CT registration alone, was shown.

Compared to existing atlas-based segmentation methods the novelty of our passive contours approach is given by implicitly incorporated information about shape and location of the organs. The general shape of the contour can not degrade (e.g. split in multiple objects) as we control the spatial regularity of the guaranteed diffeomorphic transformation by using hyperelastic regularization. Local adaptive volume regularization additionally prevents unnatural contraction or expansion of organs.

We overcome the limitation of low soft tissue contrast in CT by using additional PET images. Although the spatial resolution of PET is magnitudes lower compared to CT, the function information does not perturb the CT registration, but provides important complementary information in some soft tissue regions.

The primary goal is to apply our method to human data in future work. In addition, we will extend this work by analyzing a larger number of data sets with a larger number of VOIs. In this context it is also planned to analyze the applicability of the proposed method to subjects with tumors. It is planned to extend our method to dynamic PET data as activity over time carries important information for segmentation. An integration of our passive contour distance into the intensity-based registration of [1] is particularly promising. In future work we further plan to extend the data term to handle Poisson statistics and inhomogeneous areas as in [11].

Acknowledgments. The authors would like to thank Thomas Kösters for providing his reconstruction software EMrecon (`http://emrecon.uni-muenster.de`, [7]) used for the reconstruction of the PET datasets. This work was partly funded by the Deutsche Forschungsgemeinschaft, SFB 656 MoBil (projects B2 and B3).

References

1. Baiker, M., Staring, M., Löwik, C.W.G.M., Reiber, J.H.C., Lelieveldt, B.P.F.: Automated Registration of Whole-Body Follow-Up MicroCT Data of Mice. In: Fichtinger, G., Martel, A., Peters, T. (eds.) MICCAI 2011, Part II. LNCS, vol. 6892, pp. 516–523. Springer, Heidelberg (2011)
2. Chan, T., Vese, L.: Active contours without edges. IEEE Trans Image Process 10(2), 266–277 (2001)
3. Chan, T., Vese, L.: Active contour and segmentation models using geometric PDE's for medical imaging. In: Malladi, R. (ed.) Geometric Methods in Bio-Medical Image Processing: Mathematics and Visualization, pp. 63–75. Springer (2002)
4. Dogdas, B., Stout, D., Chatziioannou, A., Leahy, R.: Digimouse: a 3D whole body mouse atlas from CT and cryosection data. Physics Med. Biol. 52(3), 577 (2007)
5. Gigengack, F., Ruthotto, L., Burger, M., Wolters, C., Jiang, X., Schäfers, K.: Motion correction in dual gated cardiac PET using mass-preserving image registration. IEEE Trans. Med. Imag. 31(3), 698–712 (2012)

6. Hugenberg, V., Breyholz, H.J., Riemann, B., Hermann, S., Schober, O., Schäfers, M., Gangadharmath, U., Mocharla, V., Kolb, H., Walsh, J., Zhang, W., Kopka, K., Wagner, S.: A new class of highly potent matrix metalloproteinase inhibitors based on triazole-substituted hydroxamates (radio)synthesis, *in vitro* and first *in vivo* evaluation. J. Med. Chem. 55(10), 4714–4727 (2012)
7. Kösters, T., Schäfers, K., Wübbeling, F.: EMrecon: An expectation maximization based image reconstruction framework for emission tomography data. In: NSS/MIC Conference Record. IEEE (2011)
8. Erdt, M., Steger, S., Sakas, G.: Regmentation: A new view of image segmentation and registration. Journal of Radiation Oncology Informatics, 1–23 (2012)
9. Massoud, T., Gambhir, S.: Molecular imaging in living subjects: seeing fundamental biological processes in a new light. Genes Dev. 17(5), 545–580 (2003)
10. Modersitzki, J.: FAIR: Flexible Algorithms for Image Registration. SIAM, Philadelphia (2009)
11. Sawatzky, A., Tenbrinck, D., Jiang, X., Burger, M.: A variational framework for region-based segmentation incorporating physical noise models. CAM Report 11-81, UCLA (December 2011)
12. Vese, L., Chan, T.: A multiphase level set framework for image segmentation using the Mumford and Shah model. International Journal of Computer Vision 50, 271–293 (2002)
13. Wang, H., Olafsen, T., Stout, D., Chatziioannou, A.: Quantification of organ uptake from small animal PET images via registration with a statistical mouse atlas. In: MICCAI Workshop Proceedings (2011)
14. Yezzi, A., Zöllei, L., Kapur, T.: A variational framework for integrating segmentation and registration through active contours. Med. Image Anal. 7(2), 171–185 (2003)
15. Zaidi, H., Ruest, T., Schoenahl, F., Montandon, M.: Comparative assessment of statistical brain MR image segmentation algorithms and their impact on partial volume correction in PET. Neuroimage 32(4), 1591–1607 (2006)